Stress analysis of fluid-film bearings

M PÉREZ and **C THOMAZI**
Departamento de Engenharia Mecânica, Universidade Federal de Uberlândia, Brazil
S SYNGELLAKIS
School of Engineering Sciences, University of Southampton, UK

SYNOPSIS

The Finite Element Method is used to investigate the influence of the stiffness of the housing and the backing, as well as the thickness of the antifriction lining on stresses due to lubricant film pressure in two-layered precision insert bearings. These factors are expected to affect the fatigue life of the bearings. The pressure input is obtained through a conventional hydrodynamic analysis. Results for the hoop stress at the surface of the bearing as well as for the shear stress at the interface between the lining and the backing show regions of stress concentrations, which may contribute to the initiation of failure.

Key words: fluid film bearings, stress analysis, finite element method, fatigue failure.

1 INTRODUCTION

Fluid film bearings are used to guide and support elements that rotate, usually with relatively high speeds and under heavy loadings. Connecting-rod and main crankshaft bearings of internal-combustion engines, known as precision insert bearings, are usually obtained by cold-forming a strip of low carbon steel to which layers of metallic materials are bonded with the purpose of reducing friction and allowing enough conformability for accommodating the shaft.

The material of which the surface lining is made must have a low coefficient of friction to prevent seizing between shaft and bearing when metal-to-metal contact occurs. The modulus of elasticity of the lining should also be as low as possible in order to allow conformity between journal and bearing, minimizing effects due to deviations from the exact circular form, roughness, imperfect alignment, and distortions due to thermal expansion or elastic deformation.

The resultant loading on these engine bearings varies in direction and magnitude, subjecting the bearings to cyclic deformations, which may lead to surface fatigue failure of the antifriction material. This type of failure is characterised by the nucleation and propagation of cracks that cause flakes of the lining to be detached. The number of detached flakes gradually increases, reducing the area of the bearing that supports the load. In bearings lined with babbitt, the fatigue cracks propagate first through the thickness of the babbitt layer, changing direction as they approach the interface between the antifriction lining and the backing, until they propagate parallel and adjacent to the interface, within the lining material. If the lining material is not properly bonded to the backing, these cracks will propagate rapidly along the interface (1), causing the spalling out of the antifriction lining.

Any attempt to predict failure in bearings has to be based on the knowledge of the stress distribution during service. A Fourier series elastic solution for a homogeneous ring subjected to a variety of loadings was presented by Timoshenko and Goodier (2). Lang (3) extended Timoshenko's solution to enable the stress analysis of a two-layered ring.

The lack of exact solutions to more reliable analytical models, and the difficulty in obtaining experimental results, has lead to the use of numerical techniques as a means of achieving a better understanding of the problem. Ibrahim and McCallion (4) computed the stresses in a bi-metallic strip using Finite Differences and suggested that fatigue failure would be induced either at the surface of the bearing or at the interface, due to the fluctuating stresses. Hacifazlioglu and Karadeniz (5) investigated the influence of the stiffness of the housing and the backing modelling the bearing as a semi-infinite elastic solid under plane strain conditions and using four-node non-conforming finite elements. Great emphasis has been recently placed on the interaction between the solid stress and the fluid pressure fields. Such elasto-hydrodynamic analyses have been mainly concerned with the effect of the elasticity of the housing on the hydrodynamic pressure (6) but more recent work (7) has provided a valuable three-dimensional insight into stress distributions in the bearing itself.

In the present paper some preliminary stress results for a fluid film bearing submitted to hydrodynamic pressure are reported. The Finite Element program ANSYS©, Version 5.2 (8), was used to model the bearing as a ring embedded in a rigid or flexible housing. Apart from the influence of the stiffness of the backing and housing, the influence of the thickness of the antifriction lining has also been examined in detail. The latter effect has been found to be particularly significant on the fatigue life of bearings subjected to reciprocating loads. It is expected that the results of this ongoing investigation would be useful to the development of methods for the prediction of fatigue failure of fluid film bearings submitted to variable loading.

2 FINITE ELEMENT MODELLING

In the present work fluid film bearings are analysed under static loading assuming two-dimensional linear elastic behaviour. The bearings considered in this analysis consist of a steel shell lined with a thin layer of an antifriction alloy.

For all models it was assumed that there is perfect bonding of the antifriction lining to the backing, thus ensuring continuity of displacements in that region. All models were considered to be under plane strain by assuming that there is no deformation along the longitudinal axis of the bearing. According to Ibrahim and McCallion (4) this is a realistic assumption for the

length/diameter (*l/d*) ratios occurring in practice. Hacifazlioglu and Karadeniz (5) considered this approach acceptable for a pre-design.

The radial displacement is constrained along the whole external circumference for all models, Figures 1(a) and 1(b). The nodes at the interface between the backing and the housing at $\theta = \pi$ are also constrained circumferentially, as shown in Figures 1(a) and 1(b). The constraint imposed in the circumferential direction is necessary to avoid numerical problems arising from rigid body motion and to simulate the locating lug usually found in precision insert bearings. This locating lug does not allow the insert to rotate nor to move axially within the housing.

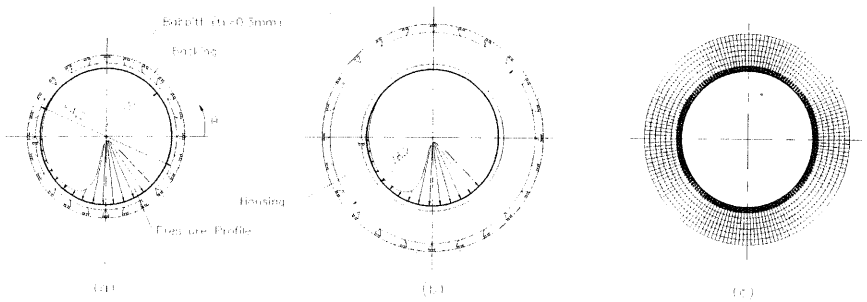

Figure 1: Geometry of bearing-housing models: (a) perfectly rigid housing, (b) elastic housing, and (c) finite element mesh.

The pressure distribution acting in the region between $\theta = 135^{\circ}$ and $\theta = 315^{\circ}$, Figures 1(a) and 1(b), was computed using Ocvirk's approach (9). An arbitrary maximum pressure $p_{max} = 10$ MPa, occurring at $\theta = 297^{\circ}$, was adopted for the analysis; this corresponded to a radial clearance $c_r = 0.022$ mm and speed of rotation $n = 3600$ rpm.
Eight-node, quadrilateral isoparametric solid elements, Plane82, were used in all models. The antifriction layer (lining), the backing, and the housing were meshed into 160×4, 160×6, and 160×6 finite elements, respectively, as shown in Figure 1(c). This meshing was adopted after running successive refinements in order to verify the convergence of results.

3 RESULTS

The model taken as a reference for comparing results had perfectly rigid housing, internal diameter $d = 50$ mm, length $l = 25$ mm, lining thickness $t_l = 0.3$ mm, and backing thickness $t_b = 1.8$ mm. These dimensions were taken from a precision insert bearing currently used in the car industry and are within the range commonly adopted for thin-walled half bearings. The antifriction metal is a tin-base babbitt with Young's modulus $E_b = 50$ GPa and Poisson's ratio $\nu_b = 0.33$ (10). The backing is made of steel, with Young's modulus $E_s = 207$ GPa and Poisson's ratio $\nu_s = 0.292$.

3.1 Influence of the housing stiffness

The elastic properties of steel (given above), cast iron ($E_{ci} = 100$ GPa, $\nu_{ci} = 0.211$), and aluminium ($E_{al} = 71$ GPa, $\nu_{al} = 0.334$), were adopted for a 12 mm thick external ring which

was included in the model (Figure 1(b)) in order to investigate the influence of the housing stiffness on the stress field in the bearing.

The radial displacement distributions at the surface of the bearing are presented in Figure 2. It can be seen in this figure that there is a change of the sense in the radial displacements in the end of the lubricated region (end of the hydrodynamic pressure region). This is due to the localised bending distortion in that region, which also generates hoop tensile stresses at the surface of the bearing. The maximum radial displacements occur under the maximum pressure, p_{max}.

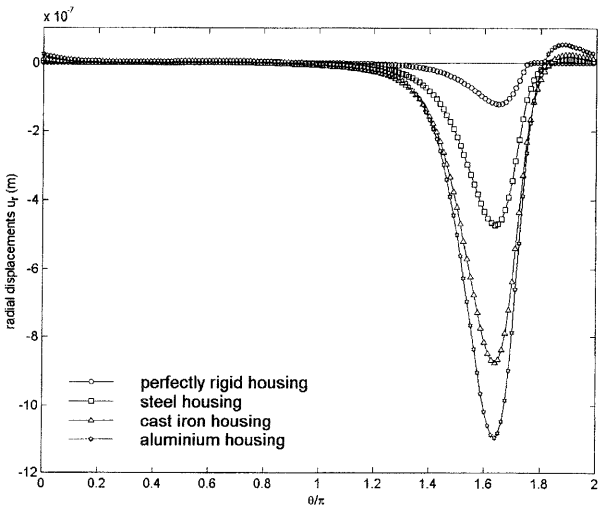

Figure 2: Radial displacements of the bearing surface.

The variation of the hoop stress, $\sigma_{\theta\theta}$, at the surface of the bearing is presented in Figure 3. For the model with perfectly rigid housing, the hoop stress is compressive over the region under hydrodynamic pressure. Its maximum value occurs at the point of maximum pressure. Although almost entirely compressive, the hoop stress becomes tensile at $\theta = 315^{\circ}$, at the end of the lubricated region, where the steepest gradient occurs. When the elasticity of the housing is accounted for, the hoop stress remains tensile over a larger region when compared to the corresponding result obtained from the model with perfectly rigid housing.

The magnitude of the tensile hoop stress increases with decreasing housing stiffness. Its maximum values through the thickness of the lining are found to be at the surface of the bearing. The maximum tensile hoop stresses at the surface of the bearing for various housing materials are presented in Table 1. The models for cast iron and aluminium housings show tensile hoop stresses within the lubricated region where the pressure gradient is high. However, the magnitudes of the tensile hoop stresses in this region are smaller than the ones determined at the end of the lubricated region (end of the hydrodynamic pressure profile).

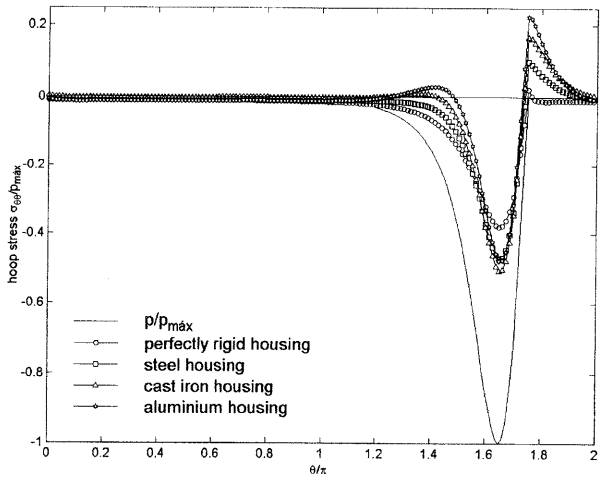

Figure 3: Influence of the housing stiffness on the hoop stresses at the bearing surface.

In all cases analysed the maximum value of the shear stress component, $\tau_{r\theta}$, in the lining occurs at the interface between the lining and the backing, under the region of the steepest pressure gradient. The maximum absolute value of the shear stress component in the insert bearing occurs, however, below this interface, within the backing. In the same way as with the hoop stresses at the surface of the bearing, the magnitudes of the shear stresses also increase with the decrease of the stiffness of the housing. The distribution of the shear stress at the interface between lining and backing is presented in Figure 4, while the maximum absolute shear stresses at the interface for various housing materials are presented in Table 1.

Table 1: Maximum tensile hoop stresses at the surface of the bearing and maximum shear stresses at the lining/backing interface for different housing materials.

Housing material	Maximum tensile hoop stress at the surface $/p_{max}$	Maximum shear stress at the interface $/p_{max}$
Perfectly rigid	0.0213	0.0303
Steel	0.0994	0.0385
Cast iron	0.1662	0.0433
Aluminium	0.2242	0.0447

3.2 Influence of the backing stiffness

The influence of the stiffness of the backing on the stress field in the bearing was also examined. The elastic properties of steel and a ceramic material (Si_3N_4) [E_c = 304 GPa, ν_c = 0.240 (11)] were used in this analysis. This ceramic material is in current use in rolling elements of antifriction bearings for machine tool spindles. The housing is considered perfectly rigid.

Comparing the model with steel backing to the one with ceramic backing it is observed that in the latter smaller tensile hoop stresses develop. Considering the housing perfectly rigid, the

maximum hoop stress for the model with steel backing is 0.0213 p_{max} while this value falls to 0.0149 p_{max} for the model with ceramic backing. The variations of the hoop stress for both models are presented in Figure 5 where the cited peak tensile stresses can be seen on the positive stress axis.

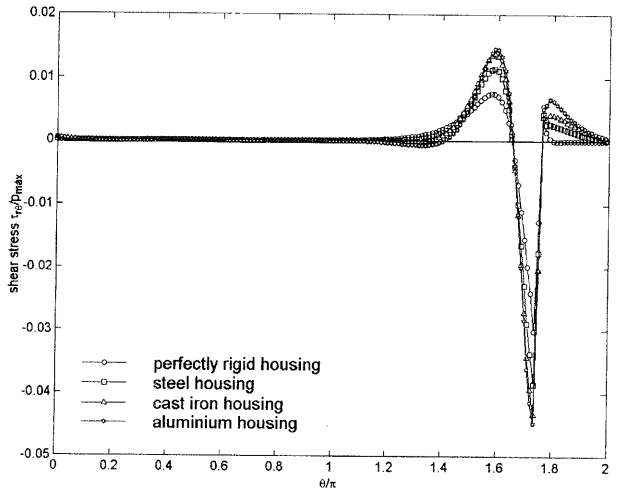

Figure 4: Influence of the housing stiffness on the shear stresses at the interface between the lining and the backing.

As can be seen in Figure 6, the maximum absolute value of the shear stress at the interface between the lining and the backing is 0.0303 p_{max} for the model with steel backing while it increases to 0.0320 p_{max} for the model with ceramic backing. The distribution of circumferential stresses in the models analysed show discontinuity at the interface between the lining and the backing. This is due to the fact that, although assuming perfect bonding in order to assure continuity of displacements, the elastic properties of the lining and the backing are different.

3.3 Influence of the thickness of the lining

The fatigue strength of babbitt alloys can be increased by laying thin layers of these materials on a steel backing. The thickness of each layer has a direct influence on the fatigue strength and on the load capacity of the bearing. It is observed experimentally that fatigue life increases with the reduction of the lining thickness (1, 10).

In the analysis to investigate the influence of the thickness of the lining on the stress field in the insert bearing the housing was assumed perfectly rigid, the bearing internal diameter was kept constant, d = 50.00 mm, as well as the thickness of the backing, t_b = 1.80 mm. Three different thickness values of the lining were adopted, t_l = 0.60 mm, t_l = 0.30 mm, and t_l = 0.15 mm. The effect of varying thickness on pressure was ignored; the applied pressure was assumed fixed under all circumstances.

The maximum values of the tensile hoop stresses at the surface of the bearing and the shear stresses at the interface between the lining and the bearing are presented in Table 2. It can be seen that both stresses decrease with the reduction of the thickness of the lining. However, the magnitude of the compressive hoop stresses increases with the reduction of the thickness of the antifriction layer, as shown in Figure 7, where the hoop stress distribution at the bearing surface is presented. The shear stress distribution at the interface between the lining and the backing is presented in Figure 8.

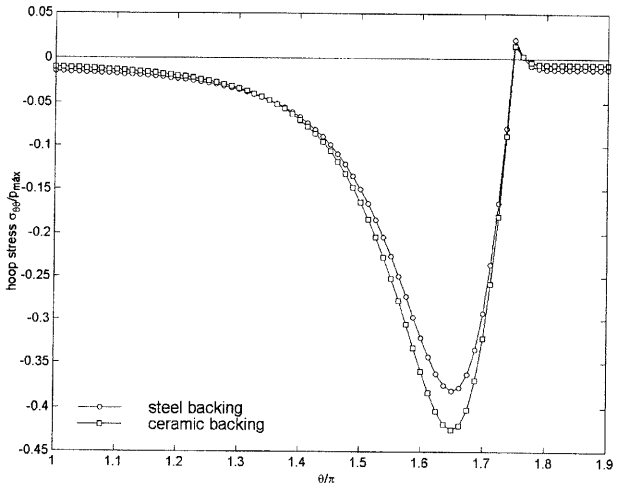

Figure 5: Influence of the stiffness of the backing on the hoop stresses at the surface of the bearing.

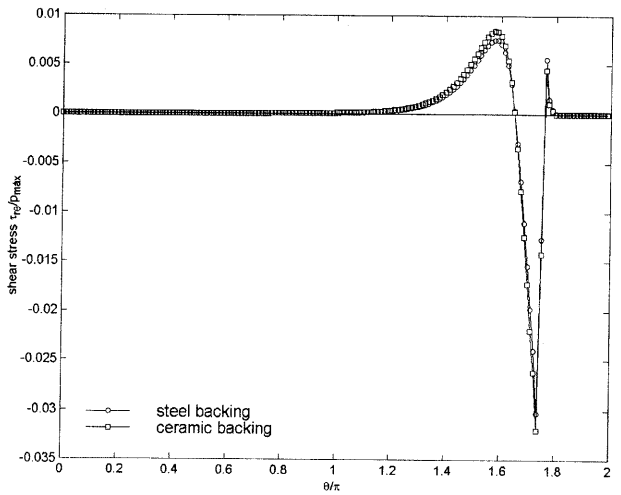

Figure 6: Influence of the stiffness of the backing on the shear stresses at the interface between the lining and the backing.

Table 2: Maximum tensile hoop stresses at the surface of the bearing and maximum shear stresses at the interface for different thicknesses of the lining.

Thickness of the lining, t_l	Maximum tensile hoop stress at the surface $/p_{max}$	Maximum shear stress at the interface $/p_{max}$
0.60 mm	0.0262	0.0512
0.30 mm	0.0213	0.0303
0.15 mm	0.0203	0.0166

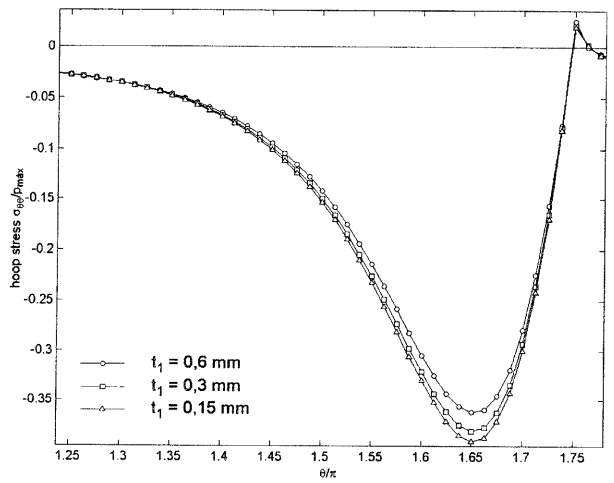

Figure 7: Influence of the thickness of the antifriction lining on the hoop stresses at the surface of the bearing.

4 DISCUSSION

Radial fluid film bearings under static loading were analysed using the Finite Element Method. The results presented in this paper give some indication of the influence that the stiffness of the housing and the backing, as well as that of the thickness of the antifriction layer may have on the stress field in a precision insert bearing.

It should be noted that the influence of residual stresses due to cold-forming as well as that of the stresses due to assembly procedures (12) were not accounted for in this analysis. Cold-forming leaves high tensile residual hoop stresses at the surface of the bearing while the stresses due to bearing spread and, particularly, bearing crush are compressive at the surface of the precision insert bearing. It may happen that the stresses due to these two causes would cancel out at the surface of the lining. However, the likelihood of this and the conditions under which it would happen deserve further investigation. No published results were found in the literature regarding the cold-forming stresses but some preliminary rough calculations indicated that the magnitude of the developing tensile residual hoop stress in the lining could be as high as the yield stress of the material.

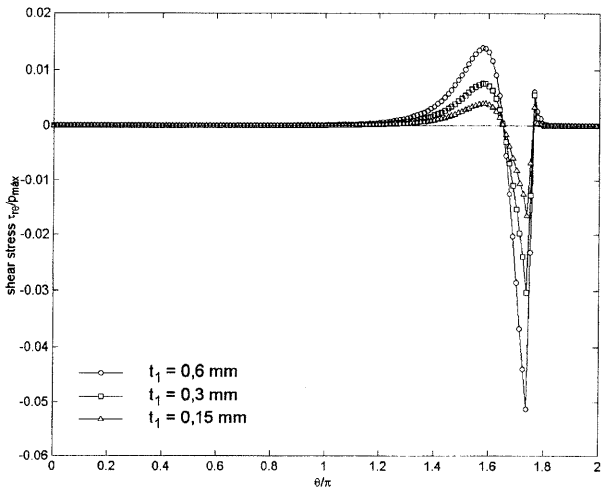

Figure 8: Influence of the thickness of the antifriction lining on the shear stresses at the interface between the lining and the backing .

Another important factor not considered in the analyses presented herein, is the influence of the deformation of the bearing and its housing on the hydrodynamic pressure distribution, which can be assessed by a coupled elasto-hydrodynamic analysis. Depending on the applied load, on the bearing/housing stiffness, and on the way the bearing had been assembled, this coupling effect on bearing stress and deformation can be significant in connection with the fatigue life of the bearing.

5. CONCLUSIONS

Within the scope of this work it is possible to conclude that:

(i) Steep pressure gradients tend to generate tensile hoop stresses at the surface of the bearing.

(ii) The magnitude of the tensile stresses at the surface and of the shear stresses at the interface rise with the reduction of the stiffness of the housing.

(iii) The use of ceramic backings reduces bending distortions due to steep pressure gradients.

(iv) The smaller the thickness of the antifriction lining, the lower the tensile hoop stresses at the surface of the bearing and the shear stresses at the interface between the lining and the backing.

The stiffness of the housing is possibly the most influential factor on the magnitude of the tensile stresses that develop at the surface of the antifriction lining. Thence connecting-rod bearings are more susceptible to fatigue failure, as they are generally less rigid than main crankshaft bearings.

Taking into consideration that the surface of the bearing is not perfect, as real bearings have surface roughness and microcracks, it may be expected that fatigue cracks should propagate from the region where the tensile stress reaches its maximum value due to operating conditions. It can also be expected that a lower stiffness of the housing should accelerate the surface fatigue failure.

As stated above, the influence of the assembly procedures on the stress field was left out in this preliminary analysis. Again, no results were found in the literature in relation to the stress distribution due to the crushing of the extremities of the insert bearings when the bearing is fitted within the housing. The solution of this problem requires the consideration of the plastic properties of the bearing/housing materials. The development of an elasto-plastic finite element solution with proper modelling of contact along the bearing-housing interface would also greatly enhance the reliability of stress predictions under realistic pressure loading.

6 ACKNOWLEDGMENTS

The first two authors are grateful to Ms. S. Rizzioli and Mr. M. L. de Oliveira, of FIAT, to Prof. C. A. de Almeida, of Departamento de Engenharia Mecânica of Pontifícia Universidade Católica do Rio de Janeiro, and to CAPES, an agency of the Ministry of Education of Brazil, for their support to the development of this work. The first author would also like to acknowledge the support received from FAPEMIG, that provided part of the computational resources that are being used for the development of this research, and to the Departamento de Engenharia Mecânica of the Universidade Federal de Uberlândia, for his leave of absence.

7 REFERENCES

(1) Wilcock, D. F. and Booser, E. R., 1957, *Bearing Design and Application,* McGraw-Hill, London.
(2) Timoshenko, S. P. and Goodier, J. N., 1970, *Theory of Elasticity,* McGraw-Hill, New York.
(3) Lang, O. R., 1977, Surface Fatigue of Plain Bearings, *Wear*, **43**, 25-30.
(4) Ibrahim, S. M. and McCallion, H., 1970, Stresses in Oil Lubricated Bearings, *Proc. Inst. Mech. Engrs*, **184**, Pt. 1, 69-78.
(5) Hacifazlioglu, S. and Karadeniz, S, 1996, A Parametric Study of Stress Sources in Journal Bearings, *Int. J. Mech. Sci.*, **38**(8-9), 1001-1015.
(6) McIvor, J. D. C. and Fenner, D. N., 1989, Finite element analysis of dynamically loaded flexible journal bearings: a fast Newton-Raphson method, *Trans. ASME, J. Tribology*, **111**, 597-604.
(7) Bahai, H. and Xu, H., 1997, Three-dimensional elastoplastic finite element and elastohydrodynamic analyses of journal bearings, *Proc. Instn Mech. Engnrs*, **211**, Pt. C, 143-152.
(8) Swanson Analysis Systems, Inc., 1995, *ANSYS Analysis Guide*, Houston, PA.
(9) Norton, R. L., 1996, *Machine Design An Integrated Approach*, Prentice-Hall Inc.
(10) American Society for Metals, 1985, *Metals Handbook*, 9th ed., Vol. 3, pp 802-822.
(11) Richerson, D. W., 1993, *Modern Ceramic Engineering - Properties, Processing, and Use in Design*, 2nd ed., Marcel Dekker, New York.
(12) Stockel, M. W., 1969, *Auto Service and Repair*, The Goodheart-Willcox Company, South Holland, Illinois.